Rare Metal Materials and Engineering
Volume 47, Issue 7, July 2018
Online English edition of the Chinese language journal

Available online at www.sciencedirect.com
ScienceDirect

Cite this article as: Rare Metal Materials and Engineering, 2018, 47(7): 2028-2036.

ARTICLE

Corrosion Resistance of TiCN Films Prepared with Combining Multi-arc Ion Plating and Magnetron Sputtering Technique

Ren Xin, Zhao Ruishan, Wang Wei, Song Xiaolong, Zhang Yang, Zhang Chongyi

Liaoning Technical University, Fuxin 123000, China

Abstract: TiCN films were deposited on AISI 304 stainless steel substrate by combining multi-arc ion plating and magnetron sputtering technique with ionizing titanium and graphite targets in an $Ar+N_2$ mixture gas. The effect of duty ratio on the microstructure and corrosion resistance of TiCN films in a NaCl 3.5 wt% solution was investigated. The results show that the as-deposited films exhibit smooth, uniform and dense morphologies, mainly forming a fcc-TiN type structure with Ti-(C, N) bond as well a as few α-CN_x, and present (111) preferred orientation with the increase of duty ratio. TiCN films display a better resistance to corrosion than the bare substrate; as the duty ratio increases, the corrosion resistance is enhanced gradually. When the duty ratio is 40%, the TiCN film shows the optimal corrosion resistance with a corrosion current density (i_{corr}) of 3.262×10^{-7} A·cm^{-2} and a polarization resistance (R_p) of 238.4 kΩ·cm^2. Electrochemical impedance spectroscopy (EIS) of the films also indicates that the penetration behavior of corrosive ions and the local corrosion process are two key factors affecting the electrode corrosion reaction kinetics process, which is consistent with the polarization curves analyses.

Key words: TiCN films; multi-arc ion plating and magnetron sputtering technique; duty ratio; corrosion resistance

Recently, TiCN films, as a mixture solid solution of TiC and TiN, are increasingly applied to the industrial, medical and decorated fields, in particular the application of tools and components, due to their increased hardness, good toughness, low friction, excellent chemical stability, corrosion resistance and biocompatibility properties[1-3]. Multi-arc ion plating and magnetron sputtering technique are two common physical vapor deposition (PVD) methods used for preparing TiCN films owing to their advantages of fast deposition rate, easily controlled deposition process and the improved film quality[4,5]. However, multi-arc ion plating may cause serious macroparticles pollution as well as obtaining poor film morphology. And magnetron sputtering technique performs the lower deposition efficiency and decreased adhesion force of the film as a result of the lower deposition energy. Additionally, taking both merits in preparing TiCN films into account, the effect of deposition process on the microstructure and properties of TiCN films has been studied, such as bias voltage[6,7], substrate temperature[8], duty ratio and discharge pressure[9,10]. Among these parameters, the duty ratio, as an important parameter of pulsed bias power, strongly influences the microstructure of TiCN films, such as surface morphology, deposition rate, growth orientation and film's density, and also further affects the film's comprehensive properties. Cheng et al[9] proposed that the increasing duty ratio of pulsed bias improved the surface morphology of TiCN coatings since the quantity of macroparticles is reduced, which presented (111) preferred orientation obviously. As pointed in the literature[11-14], the chemical composition, microstructure and corrosion resistance performance of coatings are always interrelated each other and dependent on the deposition process and conditions. However, the effect of duty ratio on the microstructure and corrosion resistance of TiCN films and the relevance between the defects and electrochemical behavior of the films have rarely been studied.

In this paper, different duty ratios were applied to depositing TiCN films using multi-arc target (pure titanium) and sputtering target (pure graphite) that were controlled

Received date: July 15, 2017
Foundation item: Science and Technology Research Project of Education Department of Liaoning Province (LJYL007)
Corresponding author: Ren Xin, Ph. D., Professor, College of Material Science and Engineering, Liaoning Technical University, Fuxin 123000, P. R. China, E-mail: lnturen@163.com

independently and co-ionized in an Ar+N_2 mixture gas. This can improve the deposition rate and the film quality, and greatly reduce the pollution of the internal structure of coating chamber, as reported in Ref.[15,16]. The microstructure of TiCN films was analyzed by X-ray diffraction (XRD), scanning electron microscopy (SEM) in combination with X-ray photoelectron spectroscopy (XPS), and the corrosion resistance of as-deposited films was investigated in a NaCl 3.5 wt% solution through electrochemical impedance spectroscopy (EIS) and polarization curves tests. After that, the effect of duty ratio on the microstructure and corrosion resistance of TiCN films in a NaCl 3.5 wt% solution was also discussed.

1 Experiment

TiCN films were deposited on AISI 304 stainless steel (SS304) substrates on a reactive ion plating system. The specimens (20 mm×15 mm×2 mm) were degreased with acetone and ultrasonically cleaned in alcohol solution and deionuzed water in an ultrasonic cleaner system for 15 min. Prior to depositing TiCN films, SS304 substrates were further cleaned with Ar^+ plasma at a direct-current bias voltage of -800 V and an argon pressure of 0.6 Pa for 3 min, and then TiCN films were deposited via co-ionizing pure titanium and graphite targets with a mixture gas of Ar+N_2. A 1:5 flow rate of Ar:N_2 was maintained by two gas flow controllers attached to the ion plating system. The duty ratio was adjusted from 30% to 60% and other detailed parameters are listed in Table 1. The deposition temperature of all specimens was 200 ºC and the distance between targets and the substrate holder was 20 cm. In order to enhance the adhesion strength of the film-substrate, a pure titanium layer of ~0.2 μm in thickness was deposited onto the substrate by sputtering the high-energy Ti^+ for 5 min in advance.

The XRD patterns of TiCN films were identified with grazing angle X-ray diffraction (XRD-6100) using Cu Kα radiation (λ=0.154 056 nm). The field emission scanning electron microscopy (FE-SEM, FEG Quanta 250) at the accelerating voltage of 10 kV was used to observe the surface and cross-section morphologies of films, and their thickness were measured with a surface profiler (XP-2) at ±0.1 μm accuracy. Supplementary details of experimental operating procedures can be found elsewhere[17,18]. The chemical composition and XPS spectra of films were obtained by X-ray photoelectron spectroscopy (PE, PHI-5400) using an Al Kα X-ray source which was operated at 14 kV and 18 mA.

The corrosion behavior of TiCN films was investigated in a NaCl 3.5wt% solution using an electrochemical workstation (Parstat 2273). Each TiCN-coated sample was enveloped and sealed by epoxy with 1 cm×1 cm exposing area. The electrochemical tests were performed using a standard three electrolytic cell including coated specimens working electrode, an saturated calomel reference electrode and Pt foil counter electrode. Prior to each measurement, all specimens were immersed in a NaCl 3.5wt% solution for 1 h to obtain a stable open circuit potential by the OCP measurement. The electrochemical impedance spectroscopy was immediately carried out at OCP with an AC sinusoidal excitation signal of 10 mV over frequency range from 1 MHz to 10 mHz and EIS results were given in the form of Nyquist and Bode plots. Simultaneously, the polarization curve test was obtained over the potential range from -0.5 V to 1.0 V with a scan rate at 0.5 mV/s dynamically. All the experiments were conducted at constant room temperature (25 ºC) and repeated for three times. According to the Tafel plot extrapolation method, many kinetic parameters, such as the corrosion potential (E_{corr}), the corrosion current density (i_{corr}), the anodic Tafel slope (β_a), the cathodic Tafel slope (β_c) and the corrosion rate, were deduced by extrapolating the liner parts of the polarization curves, and the polarization resistance (R_p) was obtained using Stern-Geary Eq.(1)[19,20].

$$R_p = \frac{\beta_a \beta_c}{2.303 i_{corr}(\beta_a + \beta_c)} \quad (1)$$

Table 1 Experiment conditions for the deposition of TiCN films

Deposition parameters	Numerical value
Arc target voltage/V	25
Arc target current/A	50
Arc target	Pure Ti metal (99.9%)
Voltage of sputtering target/V	500
Current of sputtering target/A	0.02
Magnetron sputtering target	Pure graphite (99.9%)
Pulse bias voltage/V	-300
Bias power frequency/kHz	40
Deposition pressure/Pa	0.6
Deposition time/min	60

2 Results and Discussion

2.1 Structure and chemical characterization

Fig.1 gives the change of diffraction peak intensity of TiCN films. Apart from (111), (200) diffraction peaks of the substrate Fe_γ, TiCN patterns present a cubic B1 NaCl-type structure with orientations in the Bragg planes (111), (200), (311) and (222), similar to the structure of TiC and TiN matrixes. The intensity of all diffraction peaks steadily strengthens with the increment of duty ratio and the peak is very sharp, implying that the film crystallinity is favorable[21]. However, the plane $(111)_{TiCN}$ shows the highest intensity peak among the other planes, presenting a strong textured growth along this orientation[22]. Since the plane (111) tends to have a minimal growth surface

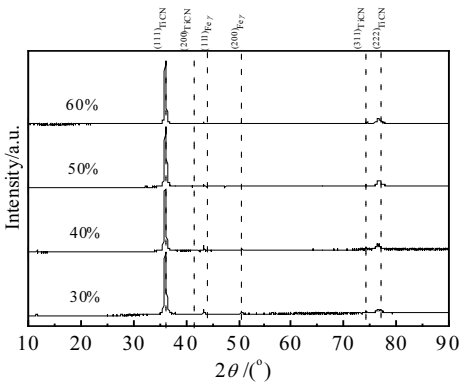

Fig.1 XRD patterns of deposited TiCN films at different duty ratios

energy during the growing of the film, the film grows toward the direction of lower surface energy so that it gives rise to the weakening or invisibility of other diffraction peaks[23]. In addition, the lattice parameters of TiCN films are determined using the Bragg law written in terms lattice parameter a:

$$\lambda = 2\sin(\theta)\frac{a}{\sqrt{h^2+k^2+l^2}} \quad (2)$$

where λ is the wavelength of the X-rays (0.154 056 nm), θ is the angle between the incident ray and the scattering planes, a is the lattice parameter, and (hkl) is the reciprocal lattice vector. As summarized in Table 2, the $a_{(111)}$ and $a_{(222)}$ lattice parameters of TiCN are similar and show a little change with the duty ratio increasing. Out of the doped carbon, the lattice parameter of TiCN is higher than that of TiN (a=0.424 nm), but lower than that of TiC (a=0.433 nm). Based on the fact that the radius of C atom is bigger than that of N atom, as the doping degree of carbon increases, some N atoms of TiN lattice (cubic lattice) are substituted for C atoms, forming a structure with substitution solid solution, which results in an asymmetric lattice distortion within the near C atoms area, increasing the lattice parameter of TiCN matrix. The crystallite sizes of films were obtained from the $(111)_{TiCN}$ and $(222)_{TiCN}$ XRD peaks at their full width at half maximum values by the Debye-Schereer formula. The average size of the grains in the TiCN films varies within a wide range of 15 ~ 25 nm (Table 2). The size of $(111)_{TiCN}$ oriented grains is much larger than that of $(222)_{TiCN}$, which can be attributed to the fact that the [111] direction is the fastest growing one in cubic structures and the crystallites with (111) plane parallel to the substrate surface are elongated along the direction of film growth[24].

According to the XPS analysis, the chemical composition of TiCN films is summarized in Table 2. With an increase of duty ratio from 30% to 60%, the C content first increases to 7.6 at% and then decreases to 6.7 at% while that of Ti and N exhibit slight variations. Since the different sputtering coefficients of Ti and C atoms, TiCN films with different duty ratios have different C contents. The higher the duty ratio, the larger the distinction of element concentrations. Moreover, the deposition rate of TiCN films was described as the ratio of the film thickness to the deposition time in the literature. It is seen from Table 2 that the deposition rate firstly increases to 3.74 $\mu m \cdot h^{-1}$ at 40% and then decreases to 3.58 $\mu m \cdot h^{-1}$ at 60% as the duty ratio increases, which arises from the ions' energy, flight speed and re-sputtering effects caused by the duty ratio. With an increase of duty ratio within a certain range, the exerting pulsed bias is prolonged, strengthening the electric field intensity of an average cycle, and improving the electric field working done for ions and the average flight speed of ions, which enhances the deposition efficiency of the films. However, when the duty ratio continues to increase, especially more than 50%, ions may carry excessive energy and intensively bombard the growing film surface, which provokes the re-sputtering effect, resulting in the reduction of deposition rate[25,26]. In addition, the intensive collision can make the substrate temperature rise and promote it.

To further get insight into the surface chemical state of TiCN films, the XPS scan spectra and core level spectra of Ti 2p, C 1s, N 1s for the samples were investigated, taking the TiCN film at the duty ratio of 40% for example (Fig.2). From Fig.2a, dominant signals of Ti, C, N, O, Ar are detected and the signals of O and Ar arise from a little residual O_2 in the chamber and the Ar^+ sputtering, respectively, as proved by the weak signal intensity out of their low content. The XPS signal (Fig.2b) includes four obvious peaks at the line position of 453.58, 456.55, 458.98, 462.14 eV corresponding to the Ti-N bond, Ti-N bond, Ti-O bond and Ti-N bond, respectively[27-29]. After doping carbon, the binding energy value of Ti $2p_{3/2}$ peak corresponding to the Ti-N bond increases and this peak position shifts to higher binding energy correspondingly. Due to a residual amount of O_2 inside the vacuum chamber during deposition, the position of N atom in TiN matrix is replaced by O atom in the form of Ti-O bond. The C 1s peak (Fig.2c) is composed of double components, and the peak lower bonding energy (283.15 eV) is assigned to C-Ti bond while the component at 285.58 eV can be assigned to the C-N bond, which can be verified by the N 1s peak at 397.78 eV[30]. Additionally, a predominant peak appearing in the N 1s spectrum at 395.29 eV from Fig.2d also confirms the presence of TiCN, which is consistent with Ref.[31]. Combining the XRD with XPS results, it is suggested that the Ti-(C, N) is the major phase in the film and some a-CN_x also exist which was undetected by XRD but observed by XPS because of a low content.

Table 2 Composition and thickness of TiCN films

Duty ratio/%	Chemical composition/at%			Deposition rate/	Lattice parameter/nm		Grain size/nm	
	Ti	C	N	μm·h^{-1}	(111)	(222)	(111)	(222)
30	44.04	5.3	50.66	3.69 ± 0.10	0.432	0.430	20.32	15.86
40	42.24	7.6	50.16	3.74 ± 0.14	0.432	0.431	20.52	15.0
50	41.35	7.12	51.53	3.66 ± 0.11	0.431	0.430	22.27	14.22
60	41.44	6.7	51.86	3.58 ± 0.13	0.432	0.430	24.4	15.7

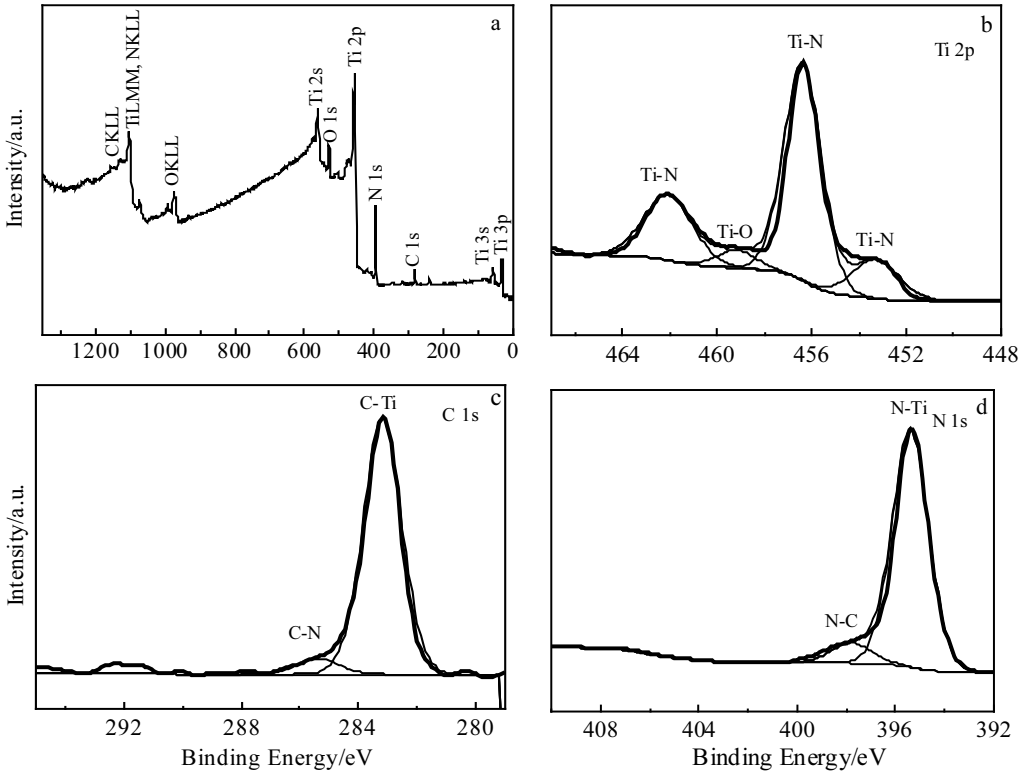

Fig.2 XPS spectra for the TiCN film at duty ratio of 40% of survey scan spectrum (a), Ti 2p (b), C 1s (c) and N 1s (d) core level spectra

2.2 Morphological characterization

Surface morphologies of TiCN films deposited under different duty ratios and the cross-section image of 40% sample are shown in Fig.3. It is clearly observed in the specimens that the surface is dense, glossy and flat, but there are still some white micro-particles, pinholes or other defects with size of less than 5 μm distributed uniformly in the films, which may stem from the effect of ions sputtering and particles ejecting, as described in Refs.[32-34]. The surface morphology of TiCN films is improved since the size and quantity of macro-particles and pinholes decrease gradually with the duty ratio escalating, as shown in Fig.3a and Fig.3b. When the duty ratio further increases, a number of cavities begin to appear because the high-energy ions intensively bombard the film surface or the bigger macro-particles fall off the film surface, as seen in Fig.3c and Fig.3d. This reveals that the surface is subjected to the deterioration and the surface roughness of films is increased, which have a negative influence on the corrosion resistance performance of TiCN films. In short, the low duty ratio can contribute to improving the surface morphology of TiCN films and the one at 40% is optimal. As displayed in Fig.3e, the as-deposited film is uniform and continuous and the thickness is about 3.7 μm. It is noted that the pure Ti interlayer can achieve a transition of physicochemical parameters from the substrate to the TiCN film, which may reduce the internal stress of TiCN films and enhance the adhesion strength.

2.3 Analysis of EIS spectra

The Nyquist plots and corresponding Bode plots of TiCN films are shown in Fig.4. As seen in Fig.4a, all specimens exhibit incomplete capacitive loops and the substrate

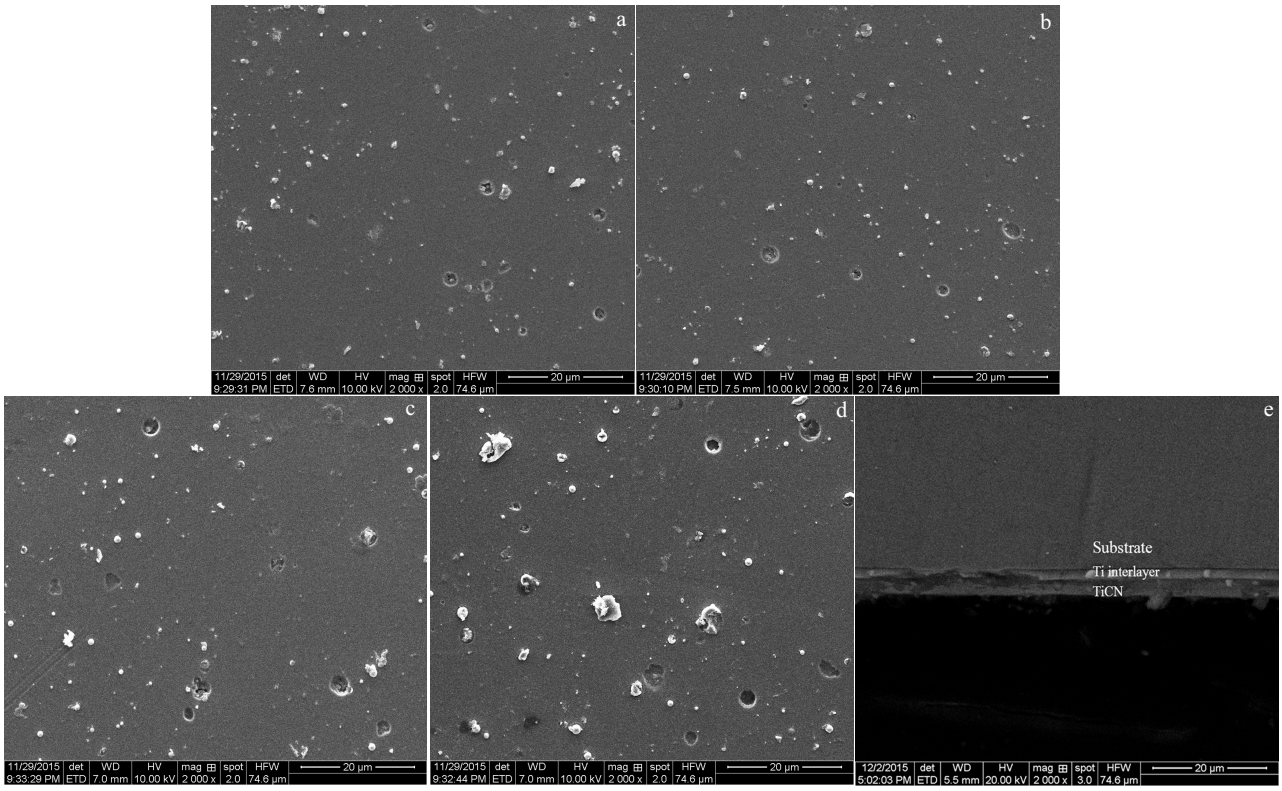

Fig.3 Surface morphologies of deposited TiCN films at different duty ratios: (a) 30%, (b) 40%, (c) 50%, (d) 60%, and (e) cross-section image of sample at duty ratio of 40%

displays the smallest diameter. Usually, the bigger the diameter, the greater impedance values and the better corrosion resistance performance of materials. The capacitive loop of TiCN films reaches the highest value at the duty ratio of 40%. It is seen that the phase angle curves (Fig.4b) obtain a wide shoulder in the frequency range from 10^{-1} to 10^{2} Hz, which responds to the double capacitive loops of Nyquist plots. The indistinct double capacitive loops in Fig.4a reveal the slight local corrosion process dominated by the micro-cells reactions of substrate/film interface due to the short exposure time (1 h) of coated samples in NaCl solution, which results in the weak response of EIS at lower frequencies. In fact, the single capacitive loop of Fig.4a is actually composed of two overlapping loops[35], suggesting that there are at least two relaxation processes responding to the state variables in the electrode reaction system.

From Fig.4b the value of log|Z| at low frequency can reflect the pros and cons of the film's ability to resist corrosion. There is a tiny fluctuation during the variation of duty ratio and the TiCN film at 40% duty ratio manifests more merits than the films with other values in the protective effects for the bare substrate. In addition, the phase angle as a function of log f for TiCN films exhibits a slow decline at lower frequencies with the increase of duty ratio, which insinuates that the materials is prone to being corroded because the corrosion medium invades preferentially from the diffusion paths of aggressive chemical species to the film/substrate interface through the protective film[36]. It is likely to giving rise to a galvanic coupling (substrate-film) in consequence of different materials' corrosion potentials when the corrosion medium exists at the film/substrate interface.

According to the characterization of electrode reaction and the experimental data in Fig.4 after Z_{simp} Win software testing, the samples can be well fitted by the equivalent electrical circuit (Fig.5a) with transient linear process of two time constants, simplified as R(Q(R(QR))), which has been used frequently to describe the AC response of the failure process of films or coatings[37]. In equivalent electrical circuit (EEC), electrolyte resistance R_s originates from the ohmic contribution between the lukin capillary mouth of reference electrode and working electrode. Constant phase angle element CPE_{po} is the film's capacitive behavior, pore resistance R_{po} is related to the films' block effect and can hinder the electrolyte penetration, which are corresponding to the response of EIS at high frequencies. Owing to the electrolyte penetration from pathways formed

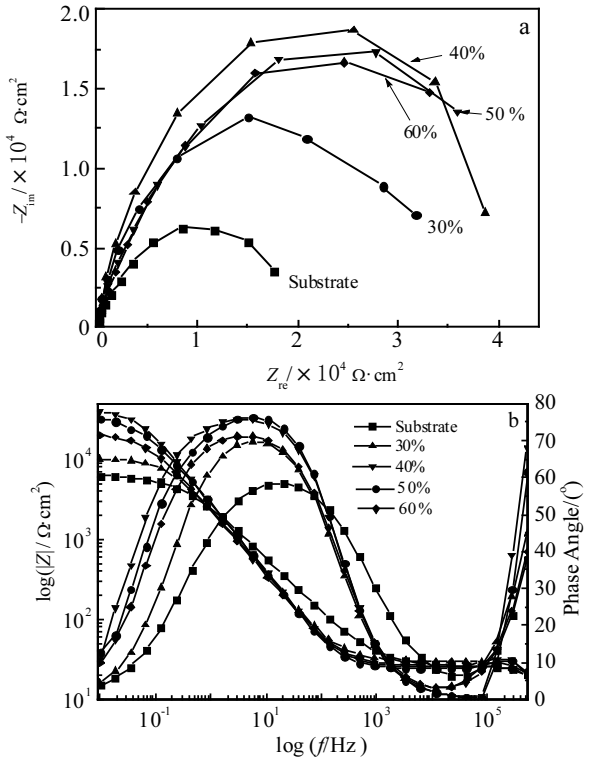

Fig.4 Nyquist plots (a) and Bode plots (b) of the substrate and deposited TiCN films at different duty ratios

by TiCN films' defects, the substrate/electrolyte interface is equal to a plate capacitor, CPE_{dl} denotes the double layer capacitance and R_{ct} is the corresponding charge transfer resistance, modeling the local corrosion process at lower frequencies. Out of the dispersion effect, constant phase element CPE or Q is used to represent a non-ideal capacitor accounting for the inhomogeneities of the material surfaces[38]. It describes the deviation from the actual capacitive behavior and its impedance can be expressed as:

$$Z_Q = \frac{1}{Y_o(j\omega)^n} \tag{3}$$

Where Y_o is capacitance, ω is angular frequency and n is dispersion coefficient, usually $0<n<1$, which explains the degree of deviation from a pure capacitor. In essence, the EEC model of Fig.5a can be seen as one consisting of Faraday impedance (Z_F) and Non-Faraday impedance (Z_{NF}), which is elaborated exhaustively in pioneer works[36]. So, the total impedance Z_t of electrode system is derived as follows:

$$Z_{NF} = \frac{1}{(Y_o)_{po}(j\omega)^n} \tag{4}$$

$$Z_F = R_{po} + \frac{1}{(Y_o)_{dl}(j\omega)^n + \frac{1}{R_{ct}}} \tag{5}$$

$$Z_t = R_s + \frac{1}{\frac{1}{Z_{NF}} + \frac{1}{Z_F}} \tag{6}$$

Thus, Z_t is ultimately expressed as (7) by integrating (4), (5) with (6) simultaneously.

$$Z_t = R_s + \frac{1}{(Y_o)_{po}(j\omega)^n + \frac{1}{R_{po} + \frac{1}{(Y_o)_{dl}(j\omega)^n + \frac{1}{R_{ct}}}}} \tag{7}$$

Based on the above-mentioned EEC, electrical parameters of the substrate and films are summarized in Table 3 by fitting procedure with the circuit of Fig.5a. Antunes et al[36] proposed this equivalent electrical circuit and simulated the electrochemical behavior of TiCN-coated 316L stainless steel in Hanks' solution. It is clearly seen that the R_{ct} of TiCN films increases smoothly from 3.04 $k\Omega\cdot cm^2$ to 4.57 $k\Omega\cdot cm^2$ due to the increased physical barriers determined by the film's microstructure, but it decreases subsequently while the R_{po} is little affected. As discussed in our previous works[39], the electrode corrosion reaction process of TiCN-coated SS304 was governed by the electrochemical reaction, i.e. electrons transfer originating from the charge transfer on the base of double layer at lower frequencies and the matter transfer process, i.e. Cl^- diffusion and transmission at high frequencies. During the initial period of immersion, H_2O, O_2, Cl^- etc. of electrolyte penetrate from the surface defects of materials but don't arrive at the interface of substrate/film, and the Bode plots (log f vs. phase angle) only reflects the single narrow peak with one time constant. With the elapsed time, the electrochemical behavior of galvanic couplings begins to affect the electrode corrosion reaction process when these corrosive ions reach the substrate/film interface. Thus, the local corrosion process gradually becomes the main factor influencing the corrosion kinetic process, performing the lower R_{ct} and the higher CPE_{dl} at lower frequencies. Indeed, C. Liu et al[40] also demonstrated that the electrochemical behavior of PVD-TiN coatings on mild steel and AISI 316 substrates was induced by the underlying metal based on the film defects. As the TiCN film is also noble, the same assumption may be done here and the results in Table 3 corroborates it. In order to observe the fitting procedure intuitively, a physical model for the EIS response of TiCN films is given in Fig.5b. The model of films is established in the light of the presence of the intrinsic defects typical of PVD processes shown in Fig.3 and the analysis of Nyquist plots and Bode plots in Fig.4. Actually, they confirm the suitability of this circuit model.

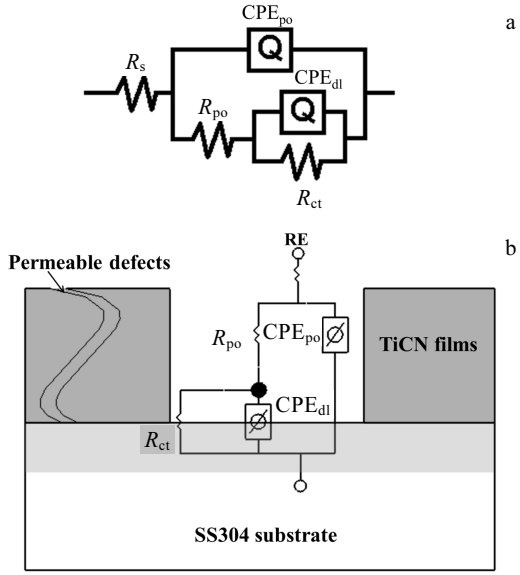

Fig.5 Equivalent electrical circuit (a) and physical model (b) of TiCN-coated samples

Based on this, it can be inferred that the film surface morphology and compactness are key factors influencing anticorrosive performance of films indirectly. As a matter of fact, the microstructure of TiCN films presents some intrinsic defects such as macroparticles, pinholes or microcracks generated in the period of deposition process. In turn, these defects may be a pathway to the penetration of the electrolyte so that it reaches the interface of film/metal substrate, causing the failure of the film protective function, which are consistent with research results of these literatures[41,42]. In spite of this, the higher R_{ct} of TiCN films reflects slower electrons transfer, i.e. low corrosion rate, further demonstrating their stronger anticorrosive abilities to aggressive ions compared with that of the bare substrate.

2.4 Potentiodynamic polarization tests

It can be seen from the polarization curves of Fig.6 and kinetic parameters of Table 4 that the electrochemical behaviors of TiCN films and the substrate are different. TiCN-coated SS304 present a more positive corrosion potential than the substrate, shifted it by only -0.186 V at the duty ratio of 40%. This illustrates that the anode reaction rate of films is retarded and needs a higher potential for moving the Cl^- across the film/substrate with freedom. Meanwhile, the lower i_{corr} and the higher R_p of TiCN films than those of the substrate imply that the corrosion rate of coated samples is lower. As the duty ratio increases, the corrosion current density of TiCN films obtains the minimal value of 3.262×10^{-7} A·cm^{-2} at the duty ratio of 40%, suggesting a homogeneous and stable structure since it doesn't dissolve, which expresses a better resistance to uniform corrosion. As shown in Fig.6, TiCN films deposited at different duty ratios exhibit a continuous and slow increase of the corrosion current density with the potential growing, but the current density near 0.74 V (30%) >1.0 V (40%), 0.79 V (50%), 0.59 V (30%) increases sharply, higher than that of the substrate (0.15 V), which is probably related to the stable pitting process occurring with the film/substrate interface due to the continuous penetration of the electrolyte that reaches the metal substrate through the permeable defects of films. This also illustrates that TiCN films present a favorable pitting corrosion resistance in comparison with the bare metal substrate. Y. Cheng et al[43] have also found that the TiCN films is effective to improve the anticorrosive property of metallic substrate. While the current density of the substrate displays a dramatic rise when the potential is 0.122 V, indicating the breakdown of passivity and initiation of pitting corrosion, which is in agreement with above discussed results.

Table 3 Characteristics of equivalent electrical circuit derived from the EIS in 3.5 wt% NaCl solution

Sample	R_s/Ω·cm^2	(CPE-Y_o)$_{po}$/×10^{-5} F·cm^{-2}	R_{po}/Ω·cm^2	(CPE-Y_o)$_{dl}$/×10^{-5} F·cm^{-2}	R_{ct}/kΩ·cm^2
SS304	26.03	-	-	9.05	6.59
TiCN(30%)	29.66	8.29	27.64	8.27	3.04
TiCN (40%)	28.51	5.50	28.39	6.78	4.57
TiCN(50%)	27.52	8.89	27.6	8.51	4.48
TiCN(60%)	25.42	9.21	24.58	8.96	3.05

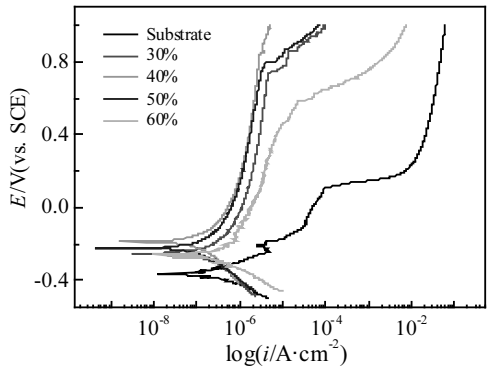

Fig.6 Polarization curves of the substrate and deposited TiCN films at different duty ratios

Table 4 Kinetic parameters of potentiodynamic polarization tests

Sample	β_a/V	β_c/V	E_{corr}/V	i_{corr}/$\times 10^{-7}$A·cm^{-2}	R_p/kΩ·cm^2
SS304	0.207	0.199	-0.358	73.62	5.984
TiCN(30%)	0.419	0.205	-0.252	4.258	140.3
TiCN(40%)	0.369	0.348	-0.186	3.262	238.4
TiCN(50%)	0.361	0.249	-0.215	3.736	171.3
TiCN(60%)	0.524	0.168	-0.265	5.48	100.8

The favorable corrosion resistance of TiCN films could be traced to its refined microstructure and fewer defects because ions possessing higher energy and speed intensively impinge these atoms and particles deposited on the substrate as the duty ratio increases gradually. This improves the film compactness and reduces permeably the activity of atoms and boosts their diffusion abilities so that reduces defects in the film. However, the film surface also exhibits more cavities and pinholes as a result of the internal stress of films and intensive bombardment to films when the duty ratio exceeds 40%. Deposition process parameters, such as substrate bias, duty ratio, substrate temperature, gas pressure, may have significant influence on the quality of coatings and be controlled in order to obtain a more refined, compact and corrosion resistant PVD coatings in Refs.[44,45]. Therefore, it is a worth thing that the anticorrosive property of metallic substrate is obviously intensified by depositing TiCN films on their surface at suitable process parameters. This finding confirms the above EIS results.

3 Conclusions

1) As-deposited TiCN films show smooth, uniform and dense morphologies, mainly forming a fcc-TiN type structure with Ti-(C, N) bond as well as a few *a*-CN_x, and present (111) preferred orientation with an increase of duty ratio.

2) The electrochemical impedance spectroscopy of TiCN films reveals that there are two constant times from EIS results, i.e. the corrosive ions' penetration of the electrolyte through the defective TiCN films at high frequencies and the local corrosion process dominated by the electrochemical behavior of galvanic couplings occupied with the substrate/film interface at lower frequencies.

3) TiCN films display a better resistance to corrosion than the bare substrate and its corrosion resistance is enhanced gradually with the duty ratio increasing, and that of films at 40% shows the optimal one with a corrosion current density (i_{corr}) of 3.262×10^{-7} A·cm^{-2} and a polarization resistance (R_p) of 238.4 kΩ·cm^2.

References

1 Takadoum J, Houmid-Bennani H, Mairey D *et al. Journal of the European Ceramic Society*[J], 1997, 17(15): 1929

2 Wang Q Z, Zhou F, Zhou Z F *et al. Surface and Coatings Technology*[J], 2013, 253: 199

3 Sedira S, Achour S, Avci A *et al. Applied Surface Science*[J], 2014, 295(5): 81

4 Yang Lijun, Zhang Zehui, Li Lin *et al. Rare Metal Materials and Engineering*[J], 2015, 44(6): 1455 (in Chinese)

5 Liu Y L, Liu F, Wu Q *et al. Transactions of Nonferrous Metals Society of China*[J], 2014, 24(9): 2870

6 Lai Q, Huang S H. *Advanced Materials Research*[J], 2011, 328-330: 1339

7 Wang Mengmeng, Huang Meidong, Pan Yupeng *et al. Vacuum*[J], 2015, 52(1): 34 (in Chinese)

8 Chawla V, Jayaganthan R, Chawla A K *et al. Materials Chemistry and Physics*[J], 2008, 111(2-3): 414

9 Cheng Fang, Huang Meidong, Wang Mengmeng *et al. China Surface Engineering*[J], 2014, 27(4): 100 (in Chinese)

10 Mei F H, Shao N, Wei L *et al. Materials Letters*[J], 2005, 59(17): 2210

11 Bin-Sudin M, Leyland A, James A S *et al. Surface and Coatings Technology*[J], 1996, 81(2-3): 215

12 Li Ying, Qu Li, Wang Fuhui *et al. Journal of Chinese Society for Corrosion and Protection*[J], 2003, 23(2): 65 (in Chinese)

13 Lin C H, Duh J G. *Surface and Coatings Technology*[J], 2008, 203 (5-7): 558

14 Zhang Xingyuan, Jiang Sichuan, Yang Hui *et al. Materials Review*[J], 2013, 27(18): 115 (in Chinese)

15 Zhang G, Yan F, Li B *et al. Applied Surface Science*[J], 2009, 255 (21): 8788

16 Xian Guang, Zhao Haibo, Fan Hongyuan *et al. Chinese Journal of Vacuum Science and Technology*[J], 2015, 35(5): 614 (in Chinese)

17 Saoula N, Henda K, Kesri R. *Physics Procedia*[J], 2009, 2(3): 1313

18 Pan Yupeng, Huang Meidong, Xue Li *et al. Vacuum*[J], 2013, 50(1): 20 (in Chinese)

19 Cao Chunan. *Corrosion Electrochemistry Principles (Third Edition)*[M]. Beijing: Chemical Industry Press, 2008 (in Chinese)

20 Fasmin F, Srinivasan R. *Journal of Solid State Electrochemistry*[J], 2015, 19: 1833

21 Xu Junhua, Cao Jun, Yu Lihua. *The Chinese Journal of Nonferrous Metals*[J], 2012, 22(11): 3123 (in Chinese)

22 Caicedo J C, Amaya C, Yate L *et al. Applied Surface Science*[J], 2010, 256(20): 5898

23 Wang Z L, Liu Y, Zhang Z. *Handbook of Nanophase and Nanostructured Materials*[M]. New York: Kluwer Acad, Plenum Publishers, 2003

24 Kuptsov K A, Kiryukhantsev-Korneev P V, Sheveyko A N *et al. Surface and Coatings Technology*[J], 2013, 216: 273

25 Gomes R M, Barros S D, Torres S M *et al. Materials Science Forum*[J], 2009, 643: 117

26 Wang H, Zhang S, Li Y *et al. Thin Solid Films*[J], 2007, 516(16): 5419

27 Jouan P Y, Peignon M C, Cardinaud C *et al. Applied Surface Science*[J], 1993, 68(4): 595

28 Escobar-Alarcon L, Medina V, Camps E *et al. Applied Surface Science*[J], 2011, 257(21): 9033

29 Dreiling I, Haug A, Holzschuh H *et al. Surface & Coatings Technology*[J], 2009, 204(6-7): 1008

30 Wong M S, Chou H P, Yang T S *et al. Thin Solid Films*[J], 2006, 494(1-2): 244

31 Strydom I L, Hofmann S. *Journal of Electron Spectroscopy and Related Phenomena*[J], 1991, 56(2): 85

32 Uchida H, Yamashita M. *Vacuum*[J], 2002, 65(3-4): 555

33 Song Guihong, Lou Zhuo, Li Feng *et al. Transactions of Nonferrous Metals Society of China*[J], 2012, 22(2): 509 (in Chinese)

34 Münz W D, Lewis D B, Hurkmans S C T *et al. Vacuum*[J], 1995, 46(4): 323

35 Cao Chunan, Zhang Jianqing. *Introduction to EIS*[M]. Beijing: Science Press, 2002 (in Chinese)

36 Antunes R A, Rodas A C D, Lima N B *et al. Surface and Coatings Technology*[J], 2010, 205(7): 2074

37 Wang Cheng, Jiang Feng, Wang Fuhui. *Corrosion Science Protection and Technology*[J], 2003, 15(4): 200 (in Chinese)

38 Liu C, Bi Q, Leyland A *et al. Corrosion Science*[J], 2003, 45(6): 1257

39 Ren Xin, Zhao Ruishan, Huang Meidong *et al. Journal of Materials Protection*[J], 2016, 49(8): 38 (in Chinese)

40 Liu C, Leyland A, Lyon S *et al. Surface and Coatings Technology*[J], 1995, 76-77: 615

41 Wang Q, Zhou F, Zhou Z *et al. Surface and Coatings Technology*[J], 2014, 253(9): 199

42 Madaoui N, Saoula N, Zaid B *et al. Applied Surface Science*[J], 2014, 312(5): 134

43 Cheng Y, Zheng Y F. *Surface and Coatings Technology*[J], 2007, 201(11): 4909

44 Gröning P, Nowak S, Schlapbach L *et al. Applied Surface Science*[J], 1992, 62(4): 209

45 Pischow K A, Adamik M, Korhonen A S *et al. Surface & Coatings Technology*[J], 1994, 67(1-2): 95

多弧离子镀-磁控溅射复合技术制备 TiCN 薄膜的耐蚀性研究

任　鑫，赵瑞山，王　玮，宋晓龙，张　洋，张翀翊

(辽宁工程技术大学，辽宁 阜新 123000)

摘　要：采用多弧离子镀-磁控溅射复合技术在 AISI304 不锈钢基体表面于 Ar 和 N_2 混合气氛下共溅射钛靶和石墨靶制备了 TiCN 薄膜，研究了占空比对 TiCN 薄膜结构和在 3.5%NaCl (质量分数)中耐蚀性的影响规律。结果表明: 所沉积的 TiCN 薄膜表面光滑、均匀致密，主要形成具有 Ti-(C, N) 键的 fcc-TiN 型结构和少量的 α-CN_x 化合物，并随着占空比的增加表现出（111）晶面择优取向。TiCN 薄膜相比于基体表现出更好的耐蚀性能，且随着占空比的增大，薄膜的耐蚀性逐渐提高。当占空比为 40%时，TiCN 薄膜表现出最为优异的抗腐蚀性能，其自腐蚀电流密度(i_{corr})和极化电阻(R_p)分别为 3.262×10^{-7} A·cm^{-2} 和 238.4 kΩ·cm^2。薄膜的阻抗谱显示腐蚀离子的渗透行为和局部腐蚀过程是影响电极体系腐蚀反应过程中的主要动力学因素，这与极化曲线的分析结果相一致。

关键词: TiCN 薄膜; 多弧离子镀和磁控溅射技术; 占空比; 耐蚀性

作者简介：任 鑫，男，1974 年生，博士，教授，辽宁工程技术大学材料科学与工程学院，辽宁 阜新 123000，E-mail: lnturen@163.com